Russian Journal of Earth Sciences Online ISSN: 1681-1208

Special Issue: "Kamchatka Earthquake M 8.8 on July 29, 2025"

Study of Seismic Activity Between the Mainshock and the First Aftershock of the Kamchatka Earthquake on July 29, 2025

I. O. Kitov[1,*], I. A. Sanina[1], I. N. Sokolova[2], and Yu. A. Vinogradov[2]

[1]Sadovsky Institute of Geosphere Dynamics Russian Academy of Sciences, Moscow, Russian Federation
[2]Geophysical Survey Russian Academy of Sciences, Obninsk, Russian Federation
* **Correspondence to:** Ivan Kitov, ikitov@mail.ru

Abstract: The high-amplitude seismic waves generated by the earthquakes with magnitudes similar to that of the July 29, 2025 Kamchatka event (M_W 8.8) create the background noise that can potentially mask any post-seismic activity during the first few minutes following the mainshock. Detection of signals from potential aftershocks buried in the coherent noise can be enhanced using a matched filter detector based on waveform cross-correlation with high-quality waveform templates obtained from historical events in the same region. The array stations of the International Monitoring System (IMS) located at regional and teleseismic distances provide one of the most effective networks for detecting seismic events globally. However, the coherence between noise signals and the sought signals, as generated by very similar sources in the same area, makes less efficient the detection methods based on noise suppression by velocity filtering such as beamforming. For the event on July 29, 2025 near Kamchatka Peninsula, the noise reduction method based on adding stochastic noise to the actual data was tested. During the initial 10-minute period following the mainshock, several reliable event hypotheses were created. These hypotheses are similar to those reported by the International Data Centre (IDC) and are based on the data from the same IMS stations. The IDC and the International Seismological Centre had not reported any events during this time frame, despite extended automatic and interactive analyses.

Keywords: Aftershocks, matched filter, noise whitening, International Monitoring System, International Data Centre, Kamchatka megathrust earthquake

Citation: Kitov I. O., Sanina I. A., Sokolova I. N., and Vinogradov Yu. A. (2026), Study of Seismic Activity Between the Mainshock and the First Aftershock of the Kamchatka Earthquake on July 29, 2025, *Russian Journal of Earth Sciences*, 26, ES2008, EDN: JEDWRH, https://doi.org/10.2205/2026es001118

1. Introduction

The immediate effect of earthquakes with a magnitude of around 9 on the global scale is the creation of a high-amplitude seismic noise with a broader spectrum. The combination of secondary seismic phases from the mainshock and primary *P*-phases from the aftershocks within the first few minutes can mask signals from any other natural or human-made events within several hundred kilometers. This phenomenon of high-amplitude noise lasts for tens of minutes, as was observed after the 2011 Tohoku earthquake (M_W 9.0) and the July 29, 2025 Kamchatka event (M_W 8.8).

The International Monitoring System (IMS) of the Comprehensive Nuclear-Test-Ban Treaty Organization (CTBTO) provides a low and quasi-uniform detection threshold worldwide. Real-time data from the IMS is processed by automatic system and then reviewed manually at the International Data Centre (IDC) with the aim to find all possible events present as related to the Treaty [*Coyne et al.*, 2012]. No aftershocks were detected by the IDC in the first 10 minutes after these two major earthquakes, and the body waves magnitudes of aftershocks that occurred during the first hour were larger or very close to 5. The lack of aftershocks during the initial several minutes could be due to physical

Research Article

Received: February 2, 2026
Accepted: May 25, 2026
Published: July 1, 2026

reasons of the slow strain-stress accommodation to the new state induced by the large-scale fault displacement or the inability of the standard detection methods to find signals in the coherent ambient noise. The latter problem is in the focus of this study.

Seismic arrays were proposed in the late 1950s as an effective tool for reducing the detection threshold of signals from the underground nuclear tests [*Sultanov*, 1998]. The main goal of an array is to suppress ambient noise in beamforming, as any other antenna would do [*Schweitzer et al.*, 2012]. The average detection gain is proportional to the square root of the number of individual sensors. Due to the requirement of the lowest possible detection threshold for the monitoring purposes under the Comprehensive Nuclear-Test-Ban Treaty (CTBT, https://www.ctbto.org/our-mission/the-treaty), seismic arrays dominate in the final configuration of the IMS with more than 30 operational primary and auxiliary array stations [*Coyne et al.*, 2012] in July 2025. The distribution of the IMS arrays and 3-component (3-C) stations is shown in Figure 1. All location and magnitude estimation procedures are unique to the IDC because the array stations are involved and CTBTO targets are underground explosions, which have source function different from that of earthquakes. Thus, IDC's estimates of m_b and M_S are different from other agencies [*Coyne et al.*, 2012].

Beamforming is an effective method for suppressing ambient noise. It does not require any a priori information about the signals, except for their range of slowness and frequency band. For repeating signals, such as those generated by aftershocks, a matched filter is optimal linear filter that maximizes the signal to noise ratio (SNR) given additive stochastic background noise [*Turin*, 1960]. The core of matched filter technique is cross-correlation of template signal with unknown signal. Detection methods based on waveform cross-correlation (WCC) have demonstrated extraordinary power to detect signals deep within seismic noise [*Arrowsmith and Eisner*, 2006; *Baisch et al.*, 2008; *Israelsson*, 1990; *Joswig*, 1990; *Schaff and Richards*, 2004]. However, signals from early aftershocks of the largest earthquakes are embedded in coherent microseismic noise. As a result, detection thresholds for these sought signals are much higher.

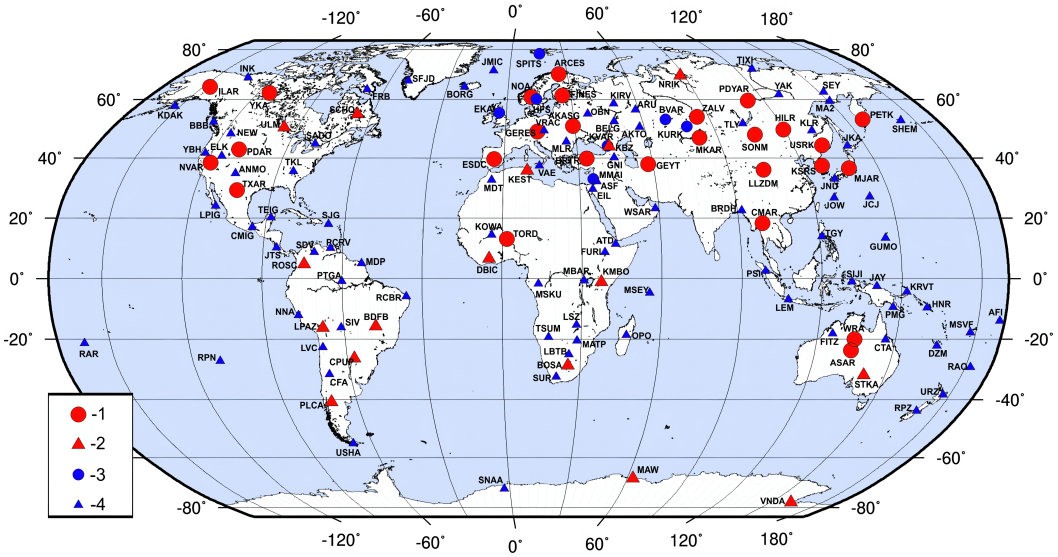

Figure 1. IMS stations. 1 – primary arrays, 2 – primary 3-C stations, 3 – auxiliary arrays, 4 – auxiliary 3-C stations.

The IDC seismic catalogue for the area around the July 29, 2025 Kamchatka earthquake is likely to be the best source of information on the following postseismic activity in this area. The presence of aftershock activity in the first few minutes after the mainshock is tested in this study with newly developed techniques that combine waveform cross-correlation with noise "whitening" by adding computer generated stochastic noise to physical waveforms [*Adushkin et al.*, 2025]. The combination of real microseismic and

digital stochastic noise effectively reduces the level of noise component that is coherent with the sought signals at the IMS seismic stations. As a result, the detection threshold is lowered and regular *P*-wave signals from the July 29 Kamchatka earthquake can be found in the first few minutes after the mainshock.

2. Data and Method

According to the CTBT, the IMS seismic network consists of 50 primary stations and 120 auxiliary stations. The number of operational stations changes over time as new stations are added. During the time period from July 1 to August 2, 2025, there were 28 primary and 6 auxiliary seismic arrays in operation. There were also several auxiliary and one primary 3-C stations at regional and near-teleseismic distances away from the Kamchatka July 29, 2025 mainshock. In this study, only data from the IMS stations is used for cross-correlation. At the IDC, a set of event hypotheses is routinely generated using a three-stage automatic process. The final result of this automatic processing is called the Standard Event List 3 (SEL3). Experienced IDC analysts then create the final version of the IDC event list – the Reviewed Event Bulletin (REB) [*Coyne et al.*, 2012] also available from the ISC with an approximately two-month delay. Selected parameters of the REB events for July and 19 days of August 2025 are listed in [*Kitov*, 2026, Appendix 1].

We produce a cross-correlation Standard Event List (XSEL) in automatic processing based on the IMS data also used by the REB. Only first *P*-wave phases (Pg, Pn, P, PKP, PKPab, PKPbc) are selected for WCC-processing as waveform templates. The official IDC bulletin is used as a reference to match by the XSEL. For WCC processing, only the REB events with associated detections are used as master events (ME) together with their waveform templates. The REB has grown incrementally since its inception in 2001, so the WCC uses the continuously increasing in the number and spatial coverage REB dataset to adjust the ME set for maximum overall effectiveness. The WCC process aims to find all the event hypotheses in the IMS data that match the set of IDC requirements called Event Definition Criteria (EDC). The most important EDC requirement is that the number of stations associated with a given event hypothesis must be greater than or equal to three. Any XSEL event hypothesis must be similar to one or more (collocated and repeated) ME(s) from the REB. The shapes of the signals of a given XSEL hypothesis must match waveform template of its corresponding ME at three or more IMS station(s). The match must be confirmed by a predefined set of cross-correlation quality criteria. This similarity in shapes allows more information to be extracted from the signals than in standard energy detector.

As the IMS station set is the same for the XSEL and REB, we can compare the two bulletin detections directly. The match occurs when two detections at the same station are within 20 seconds of each other in two different bulletins. This 20 second window is related to an interactive procedure for arrival retiming with a maximum of 10 seconds without creating a new detection. This allows for uncertainty in the arrival time for a given detection, and as both the XSEL and the REB detections are allowed to be retimed, the maximum spacing between two detected signals can be up to 20 s. The number of matches required depends on the specific bulletin. As the XSEL bulletin is automatic, then one matched signal is enough to declare that the XSEL automatic event matches the REB event as per the IDC adapted rule. The XSEL hypotheses can match one (or more, if the REB event hypothesis by mistake consists of signals from two physical events) REB (SEL3) event or to be new to the REB. These two cases are both important, as the XSEL event hypotheses often have more associated phases than the matched REB events and thus improves them. The set of "new to the REB" hypotheses extends the REB catalog by reliable (REB-ready) event hypotheses. In addition, the absence of XSEL hypotheses matching a given REB event indicates that the latter is likely false.

The creation of XSEL hypotheses involves associating available detections from all seismic stations with potential sources, characterized by their origin times, hypocenters, and magnitudes. The process uses the relative station contributions to determine the probability that a detection to be associated with a virtual source. For the local association

(LA) process, a grid of virtual source locations is created around the corresponding ME. The grid is characterized by its radius and the spacing between virtual nodes. The empirical travel times from the ME to the IMS stations are taken from the REB to predict the travel time instead of the theoretical travel time curves such as ak135 velocity model [*Kennett et al.*, 1995]. For each node, the empirical travel times to the ME associated stations are corrected for the relative node position. To all associated phases, the IDC requirement of 2 seconds origin (travel) time residual is applied. This is a very strict rule for automatic processing, which relies on highly accurate arrival time estimation made by the WCC detector.

A few of the best stations are required to make an event hypothesis statistically significant. The probabilities represent the weights of the stations in the event hypotheses, and the sum of all the station weights of all associated phases defines the statistical significance of the hypothesis similar to the process at the IDC. The REB event creation is based on the EDC that were carefully estimated through the trial and error process involving a large number of experts prior to the IDC starting its work. The EDC are derived from the set of detections obtained by IMS stations according to a detection procedure adapted by the IDC [*Coyne et al.*, 2012]. The XSEL detections differ from those on the IDC list at the same IMS stations and thus the event hypotheses differ for the same physical event.

The detection efficiency of an IMS station in relation to events in the Kamchatka seismic region can be estimated using the REB over the entire period of seismic observation since 2001. The number of IMS stations has been gradually increasing since 2001 and the detection threshold of the IMS seismic network has been decreasing accordingly. The long-term estimates of the station contributions are likely to be skewed, and better estimates can be made by using more recent data. Figure 2 shows the contribution of the 20 top stations to the REB in the Kamchatka seismic region. There are two time periods: (a) the full set of observations from 2001 to 2025; (b) the recent period from 2023 to 2025. The set of stations also differs, as new, highly efficient array stations such as Peleduy PDYAR (59.66°N, 112.44°E) have recently joined the IMS network. The relative contribution can be estimated against the total number of events found by the IMS network in the studied area over a specific time period, or the number of events found by the best-performing station during the same time period. Both time periods and relative figures are shown. The set of 20 top stations with a relative contribution above 0.3 to 0.4 remains relatively stable across both time periods.

Both the detection and the LA procedures used in the WCC-processing are described in several papers [*Bobrov et al.*, 2014; *Bobrov et al.*, 2016a,b]. The WCC detector relies on the matched filter approach as the signal-to-noise ratio for the cross-correlation time series is used. Ambient microseismic noise is far from meeting the matched filter requirements to be additive stochastic. Noise properties are particularly important for the cases such as the Kamchatka largest earthquakes. The earthquake-generated noise and sought signals are coherent to the extent of full shape similarity as emitted by practically collocated events with similar source functions and magnitudes. Beamforming-based detection suffers from problems, as noise suppression is not possible. Cross-correlation-based detection also fails when the shapes and amplitudes of the sought signals are similar to a large number of "noise" signals. The method fails to distinguish between the valid and "noise" signals as they are identical. There is an opportunity to suppress such coherent noise using digitally generated random time series [*Adushkin et al.*, 2025]. The essence of the method is the different effect of an added stochastic component on the coherent noise and sought signal with a slightly larger amplitude. The digital stochastic component destroys the coherency and suppresses correlation between the noise and template as required in the matched filter detector.

A stochastic noise time series, with an amplitude approximately equal to the amplitude of the coherent to the sought signal component in the noise, reduces the cross correlation with the template, say, by a factor of 2. This causes the long-term-average (LTA), in the trace

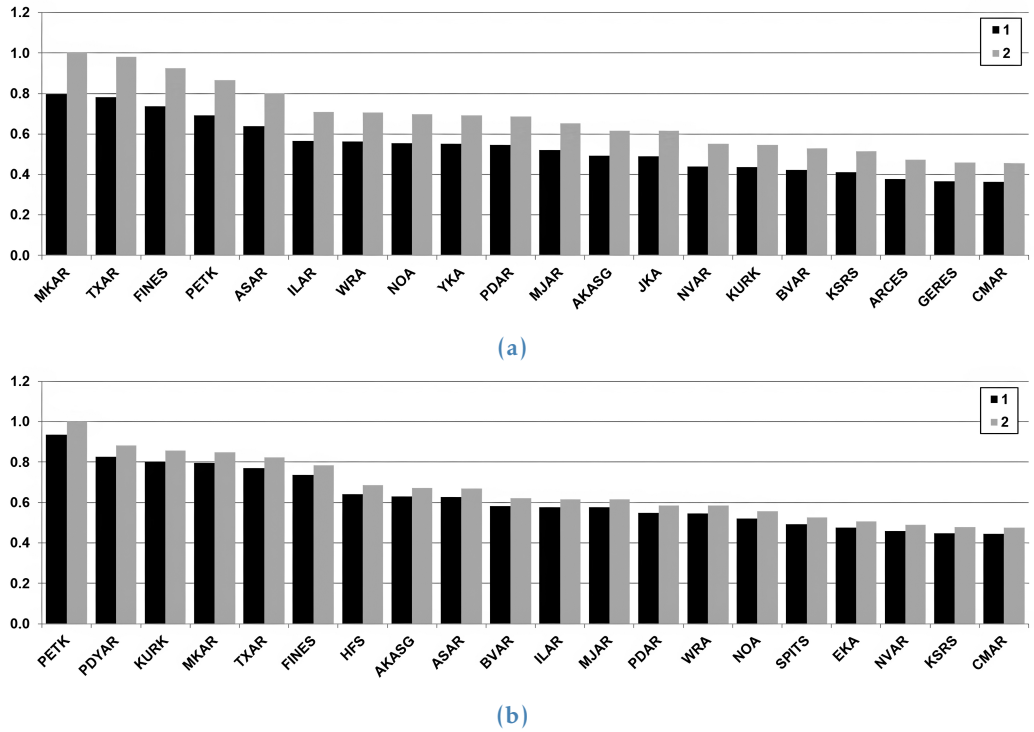

Figure 2. Relative input of 20 IMS top stations to the REB bulletin for the region 45°N–65°N, 145°E–165°E, (a) period 2001–2025, (b) period 2023–2025. All inputs are normalized to: 1 – total number of events during the corresponding period in the designated area; 2 – number of the best station with the largest input.

of cross-correlation coefficient (CC), to fall also by a factor of 2 on average. If the sought signal has a standard SNR of ~2.5, the addition of this same stochastic time series will not reduce the CC to the same proportion of noise as extensive modeling with controlled noise and signal shows [*Adushkin et al.*, 2025]. As a result, the STA in the CC-trace drops by a factor of 0.2 compared to the "no stochastic noise" case. The overall gain in the STA/LTA ratio used as SNR_{cc} can be larger than 2. It is possible to use different stochastic noise coefficients (StN) in WCC-processing and tune to the level of the coherent noise. For example, from StN = 0 to StN = 10. The variation of the microseismic noise amplitude can be represented by STA or LTA, which has also to describe the variation of the coherent component. Each sought signal and the pre-signal microseismic noise have to find the StN value to maximize the corresponding SNR_{cc}.

Detection of similar signals using the WCC is a relatively simple process. The main challenge, as with any signal detector, is to set a detection threshold that balances the flux of valid signals with false detections. Seismological agencies must conduct a thorough analysis to resolve the dilemma of valid and false events. The risk of missing the CTBT-related events leads to the IDC being relatively biased towards producing potentially false events in automatic processing. An interactive component of the process is needed to eliminate false event hypotheses and create extra event hypotheses missed in automatic processing. Approximately 50% of SEL3 events are promoted to the REB, making approximately 60% to 65% of the total number, while another 35%–40% are added by analysts in the interactive review.

The problem of detection threshold has only one solution – the trial and error method. We must calculate detection lists with various detection thresholds, associate all detections with a set of XSEL event hypotheses, then review all obtained hypotheses interactively. This process was tested at several examples and showed excellent result of the XSEL [*Bobrov et al.*, 2014; *Bobrov et al.*, 2016a,b]. Between 50 and 100 percent of new events were added

to the REB during interactive review, adapted by the IDC, when the XSEL was used instead of SEL3.

We constrain the detection flux density in the WCC-processing to the range from 30 to 120 detections per hour. The best flux density maximizing the target function of the REB matching rate has to be determined. The rate below 30 detections per hour may miss valid detections and detections spaced by 20–30 s may result in a higher rate of false events, which are not only waste of time but also are able to harm the creation of valid event hypotheses. The target function of the WCC processing is to match all REB events and to generate extra REB-ready event hypotheses with the statistical significance not worse than have the poorest REB event. The quality of XSEL events is also important for interactive analysis.

The IDC processing demands the depth estimation to be especially strict, since depths below 10 km belong to the population of natural events. Uncertainty in depth estimation plays a crucial role in ensuring that an event has a very high probability of being deeper than 10 km. When the upper bound of uncertainty is above 10 km, the event's depth is fixed at the free surface. Such events require further review and analysis. The population of REB events has significant proportion of zero depth events with shifted epicenters. For example, events potentially having depth of 700 km but a large depth uncertainty may be shifted by 10° on the surface compared to their true deep hypocenters. The WCC-based processing fixes the depths of the sought events to the depths of their ME. Additional depth correction is possible by using WCC to detect the depth phases (pP, sP, PP, PcP, Lg, etc.) when corresponding phases are available for the given ME.

The interactive review is not available for the Kamchatka earthquakes of 2025, and another procedure is used to adjust the detection and phase association processes to maximize the number of matched REB events in the XSEL. Many parameters are tuned in this process, including detection thresholds for both SNR_{cc} and standard SNR, the size of the search area around the corresponding MEs, thresholds for event weights, the minimum number of associated stations, and the minimum SNR_{cc} required for an event at one of the best stations (see, Figure 2), as the SNR_{cc} value corresponds to the probability for a detection to be valid. In addition, a set of MEs for the region under study can be selected from the full REB catalogue according to various criteria. One of the most important criteria is the distance between MEs. First of all, they should not be too far apart to avoid the gaps in sensitivity and resolution of the WCC method [*Arrowsmith and Eisner*, 2006; *Baisch et al.*, 2008]. At the same time, close MEs often produce similar event hypotheses and then elaborated conflict resolution (CR) procedure has to be used in order to select the best. The CR procedure is a part of the overall WCC-based processing and has its own parameters to determine the final XSEL event sets.

There is a standard list of MEs used in the prototype WCC processing at the IDC. These ME were selected according to a strict WCC procedure of comparing all sources one-to-one within 2° degrees around the 25000 nodes that cover the whole globe, with an average spacing of 1.25°. The best ME for each node must to be closer to it than to any other. The distance between MEs in adjacent nodes can vary from ~0° to more than 1.25°. The best 982 MEs are selected in narrow depth ranges of 40 km: 0–40, 40–80, ..., 680–700 km using the same global grid. The maximum depth for seismic sources is fixed at 700 km. Panel (a) of Figure 3 shows a schematic of this subset of MEs within the region of interest. In panel (b), we selected the top 100 MEs from the routine set that cover the area and depth range from 0 to 700 km [see, *Kitov*, 2026, Appendix 2]. The epicenters of the two mainshock events on July 20 and 29 are also shown, both located at zero depth and close in space.

The optimization procedure provides the best set of parameters used in routine processing of IMS data depending on the flux of events. During the time periods with several events per day separated by at least tens of minutes the LA procedure is simple as each ME has to produce a detection list without overlapping of the arrivals from different sought events. There is no conflicts between different physical events for the same physical

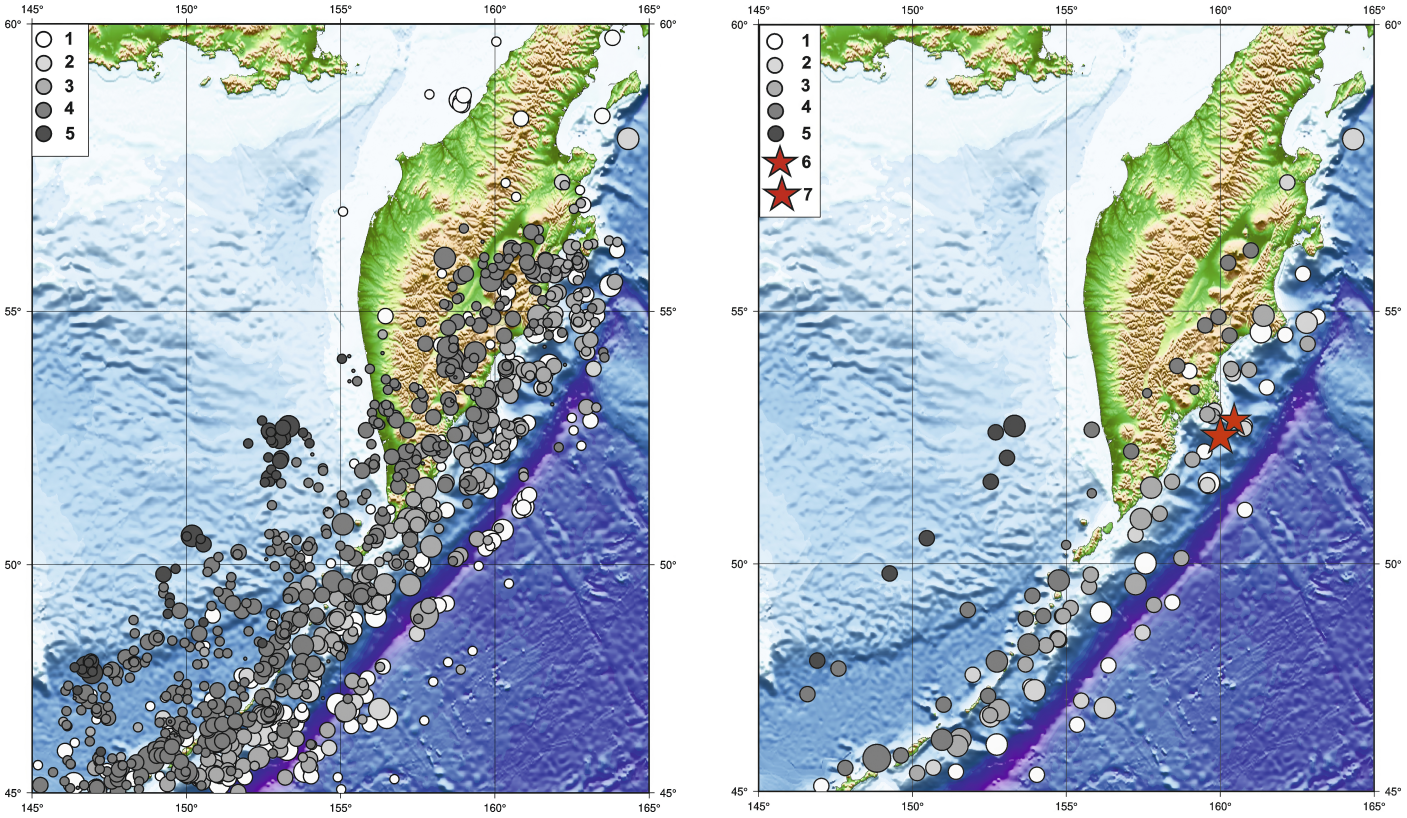

Figure 3. Master events. (a) The set of MEs used in the IDC prototype WCC-processing; (b) 100 MEs used in this study. Size proportional to m_b. Depth: 1 – $h = 0$; 2 – $0 < h \leq 40$; 3 – $40 < h \leq 80$; 4 – $80 < h \leq 410$; 5 – $410 < h \leq 700$. 6 – event 20.07.2025; 7 – 29.07.2025.

arrivals. The time period just after the earthquake of $M_W = 8.8$ contains signals from various segments of the mainshock with duration of ~90 s together with possible immediate aftershocks, though not found in the IDC processing. The detection lists for a given ME have to include arrivals of almost simultaneous events at short distances from each other and also arrivals from distant events having different propagation paths to stations but arriving at approximately the same time. The LA procedure meets numerous conflicts between different events for the same detections. When one of competing event hypotheses wins (in the order: event weight, number of associated stations, and RMS origin time residual) the given arrival all other competing hypotheses lose it together with its weight and other event defining parameters. For a given losing event hypothesis, the total loss should not exceed the set of predefined thresholds. The strict procedure is simple – one lost phase is enough to reject this hypothesis. This works excellently during seismically quiet periods with sparse distribution of events in space and time. The soft approach allows losing up to 10–15 associated arrivals. This is needed when the detection flux for a given ME is very dense.

3. Results

The first step in the study of the Kamchatka earthquake that occurred on July 29, 2025, was to analyze the earthquake which occurred on July 20, 2025. It was also a relatively large earthquake with M_W(NEIC) = 7.4, m_b(IDC) = 5.69, IDC epicenter 52.847°N, 160.588°E, depth 0 km, and origin time 06:48:59.53. There was also an event (52.909°N, 160.452°E, depth = 0 km) with $m_b = 5.39$ and M_W(CSEM) = 6.7 at 06:28:14.22 UTC, which could be considered as a foreshock, and an event (52.722°N, 160.755°E, depth = 0 km) with $m_b = 5.96$ at 07:07:41.02 UTC, which has larger m_b than the mainshock, but lower M_W(CSEM) = 6.6.

After the July 20 mainshock (M_W = 7.4), there was a 7-minute gap in seismicity till 06:56:01.43. The same gap is reported by the ISC [*ISC...*, 2026] with slightly different origin times as related to the depth difference between the IDC (fixed to 0 km, and thus, earlier in time) and ISC (34 km and 10 km, respectively) solutions.

Figure 4 presents the IDC history of the events around the Kamchatka Peninsula region from January 1 to August 19, 2025. The IDC provides body wave magnitudes with the known effect of the magnitude distribution saturation near the level of 6.0 to 6.5. In this study, m_b(IDC) is used as we search for events with unbiased magnitudes around m_b = 5–5.5. The event on July 20 has a short aftershock sequence, which practically stopped, before the July 29 earthquake. Figure 5 shows the daily number of events in 2025. The Omori law is working perfect for the July 20 aftershock sequence and has a potential kink near the day of August 10 for the July 29 sequence.

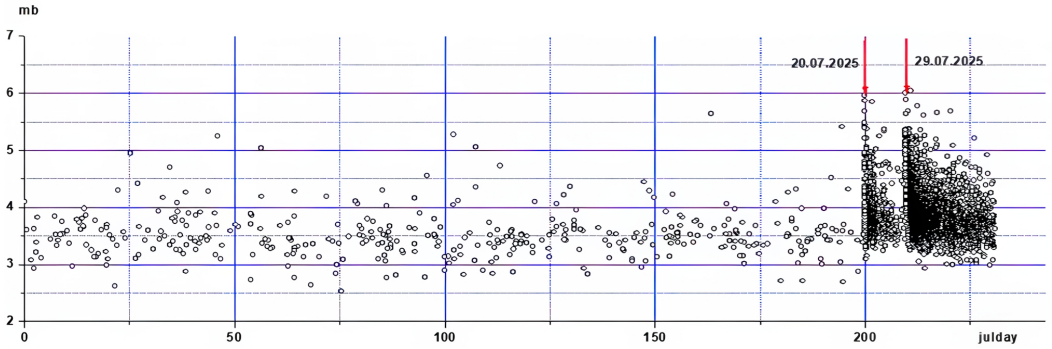

Figure 4. The evolution of seismic process in 2025 as per the REB. Region 45°N–65°N; 145°E–165°E.

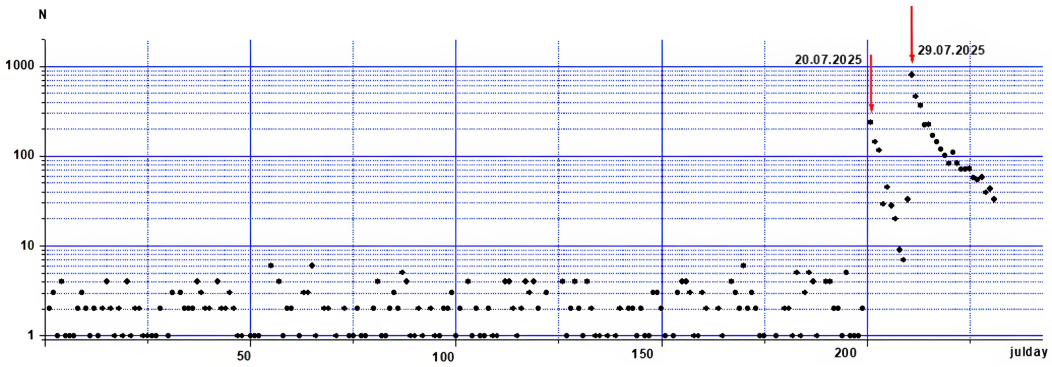

Figure 5. The number of events per day in 2025 within the region in Figure 3.

The time gap between the mainshock and the first found aftershock is 422 s for July 20 and 600 s for July 29 as shown in Figure 6, with the July 20 gap sequence showing potential periodic features, while July 29's sequence has much weaker periodicity. The following aftershocks sequences have significantly shorter time gaps. The average gap for the 30 immediate aftershocks is 105 s and 63 s for the July 20 and 29 sequences, respectively. The July 20 sequence also demonstrates a few intervals with linearly growing gaps, e.g., the aftershocks with order numbers 7 to 11 and 12 to 15 in Figure 6. Figure 7 shows that such a behavior can be related to the magnitudes of the events in the beginning of the gaps starting with the event at 06:28:14.22.

The aftershocks sequence of the July 20 earthquake reported by the IDC was compared with different versions of the WCC-based processing in order to tune the set of defining parameters to match the REB. The focus was on the 60 to 90 minute period after the mainshock, characterized by the highest aftershocks occurrence rate. The standard version of the WCC detector uses the time series of the cross-correlation coefficient, CC(t), averaged over channels as calculated for 3-C and array stations, to detect signals from the aftershocks. The WCC-detector is applied to the CC(t) and standard STA/LTA (SNR_{cc}) approach declares

a detection when SNR_{cc} is above the predefined threshold, which, in turn, is estimated from the long-term seismological observations for any given place. (Standard SNR is also calculated by a procedure similar to that adapted by the IDC and compared with the related IDC estimates where available as presented in corresponding Appendices.) We gradually decrease the threshold for each station, running the WCC detector and LA process in the same time interval. The resulting XSELs are compared to the REB in order to select an optimal set of threshold values. High thresholds miss many valid arrivals and result in a low number of XSEL events. Lowering thresholds increases the number of detections together with the number of XSEL events. The number of matched REB events also grows. At some point of low thresholds, the number of detections reaches the level when they interfere and negatively affect the LA creating too many conflicts. When such degradation is first found the previous threshold level is considered optimal.

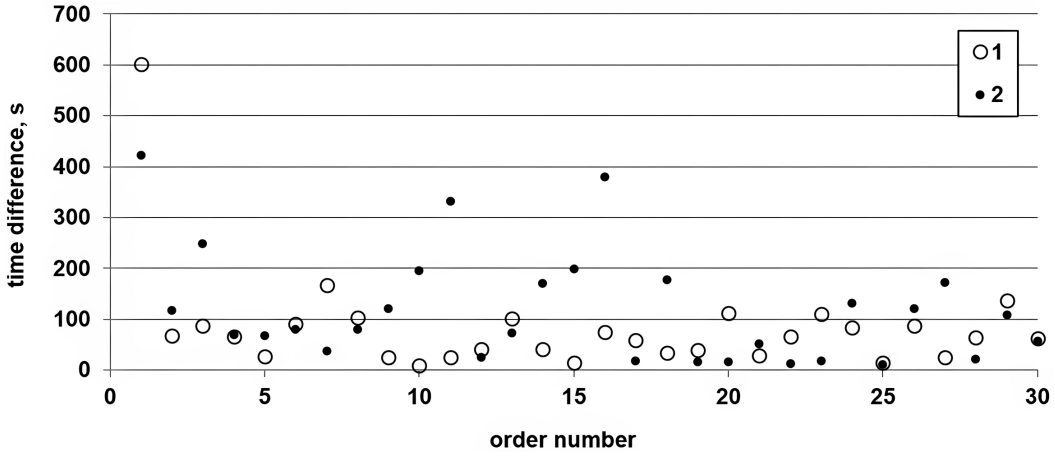

Figure 6. The time gaps after each of the thirty events following the July 20th and July 29th 2025 mainshocks. Gaps after the two mainshocks were 422 s and 600 s, respectively. 1 – July 29th (average difference 63 s); 2 – July 20th (average difference 105 s).

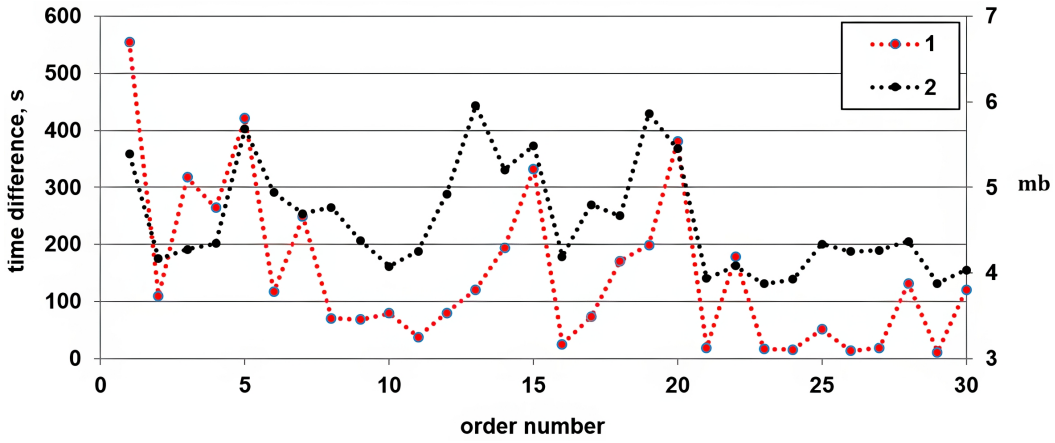

Figure 7. Comparison of time gaps between subsequent events of the July 20 earthquake starting with the event at 06:28:14.22 UTC. 1 – time intervals; 2 – m_b.

For the July 20, 2025 earthquake, the optimal set of thresholds and LA parameters was used in the routine WCC-based processing. The final XSEL contains events matching all 42 events from REB between 06:00:00 and 07:59:00. In [*Kitov*, 2026, Appendix 3], a list of matches is presented for the processed time period with the MEs providing the best match. It is worth noting that the majority of the XSEL events are those with an equivalent in the REB, since they have a similar number of associated stations. The REB events can be divided into two groups by their source of creation: 28 events were created

from SEL3 seeds (defined by the same event ID in both bulletins) and 14 events created by analysts using different methods from scratch. The latter group is also fully matched in the automatic XSEL bulletin. Moreover, in the second group, many events have more associated stations in the XSEL than in the matched REB events. There are several such examples in [*Kitov*, 2026, Appendix 4], where the REB events have 4 or 5 associated stations and the corresponding XSEL events have 8 and 9, respectively. Due to lack of SEL3 seeds and ad hoc procedures, interactive review may be imperfect. It potentially misses valid events in the REB, which are found by the WCC routine processing. For this study, the main result of the standard WCC processing is that there were no new events in the XSEL between the July 20 mainshock (M_W = 7.4) and its first aftershock. Therefore, noise reduction techniques may need to be used to find such events in the IMS seismic data in any.

The WCC-based cross-correlation with stochastic noise was carried out for a short time interval between 06:00:00 and 7:43:00, as the StN values varied from 0 to 50 with various increments. The range of StN values is obtained from the previous experience and from an extensive testing before the final calculations. The full StN set is applied to each IMS station as the noise changes significantly and the best value is difficult to foresee. Each StN value requires a full calculation process, which is costly when 10 to 20 StN values are used. The detection rate increases with StN value and the detection threshold must be increased to maintain a detection flux between 40 to 80 per hour (i.e., 45 to 90 second intervals between successive arrivals on average). Therefore, a series of complete runs is needed to adjust the SNR_{cc} thresholds to allow the desired detection flux and to achieve the best match for the REB events.

The July 20 earthquake allowed us to test at a smaller scale the advantage of noise whitening in finding reliable event hypotheses before the first aftershock. [*Kitov*, 2026, Appendix 5] lists the XSEL events that occurred between 06:48:00 and 06:57:00. The XSEL contains three new event hypotheses that were created during this time period and matched the EDC. These new hypotheses were not surprising, as the 14 REB events created by IDC analysts with similar statistical properties were also matched in the XSEL. Therefore, the mainshock with M_W = 7.4 had a 420 second no-IDC-event period before the first aftershock possibly due to the high-amplitude coherent noise from the mainshock.

The final stage was to find events occurring within the first ten minutes after the mainshock of the July 29 event. The rate of the REB events matches was a secondary objective, as an increasing number of low-amplitude detection needed to find events deep in the high-amplitude noise is able to destroy some weak and very close in space and time events in the CR procedure. The WCC processing was conducted with added stochastic noise in the time period between 23:00 on July 29 and 01:00 the following day. A full range of the StN and both parameters representing the ambient noise – STA or LTA were used. Parameters affecting the detection rates at CC-traces at involved IMS stations were also varied in a wide range, with SNR_{cc} threshold as the most significant. As the optimal set was not known in advance, a trial and error method was used to find the most efficient set. Following a comprehensive analysis, LTA was selected and a SNR_{cc} set guaranteeing a detection rate of ~60 per hour was determined. This rate was close to that of the REB events following the first aftershock – 24 events between 23:34:49 and 23:59:31. There were 43 REB events during the first hour of July 30 and 54 during the second hour.

In the optimal WCC processing case, six XSEL events new to the REB were found within 10 minutes after the mainshock. [*Kitov*, 2026, Appendix 6] presents the XSEL for this period between the July 29 mainshock and its first aftershock. The earliest new event, at 23:26:33, can be related to the stopping phase [*Savage*, 1965]. The origin time corresponds to the end of an ~90-second rupture. The epicenter located at 47.995°N, 152.626°E, close to the end point of the rupture, and the depth of 157 km is not far from the rupture plane. The estimated m_b = 6.35 is reasonable given the noise level from the mainshock. Further investigation is needed to confirm that this event occurred and its parameters are accurately estimated. The other five events have lower magnitudes, the best (see, Figure 2) associated IMS stations, including the closest array PETK with the

highest station weight of 1.0. These events occurred at different depths and locations. The best-quality XSEL event from these six has 9 associated stations. SNR_{cc} values for the new XSEL events are similar to those of the XSEL event matching the REB event at 23:34:49.16. Therefore, the quality of the new-to-the-REB XSEL events is comparable to that of the event matching the first aftershock. The REB events in [*Kitov*, 2026, Appendix 4] also have poor IDC arrivals and low SNR_{cc} values making the quality of the new XSEL events comparable with many valid REB events.

4. Conclusion

The problem of the immediate aftershocks of catastrophic earthquakes of magnitude above 8.5 is important for seismology and tectonophysics. Seismological methods have to be able to find signals from real events despite the ambient noise conditions. The relaxation of the pre-stressed geophysical medium during and immediately after the stopping of the largest possible event compatible with the size of the Earth cannot be described correctly if the largest aftershocks are not located and their dynamic parameters are not accurately estimated. There are no aftershocks reported by the IDC and ISC during the ten minute interval following the mainshock. Standard detection and phase association methods adapted by these organizations are not able to detect signals amid the high-amplitude seismic noise generated by the mainshock and by potentially missed immediate aftershocks with the magnitudes close to that of the mainshock. Even standard WCC-based methods fail to find such detections for valid event hypotheses to be created.

The WCC processing can be enhanced by adding digital stochastic noise to raw data before waveform cross-correlation is calculated. The added noise has to match various conditions for each potential signals and thus its amplitude has to be varied in a wide range of values. The ambient noise can be represented by different parameters from a constant for the entire studied period to LTA or STA. The ambient noise is modulated accordingly, and each valid signal can potentially find almost optimal conditions for detection [*Adushkin et al.*, 2025].

The July 29, 2025 Kamchatka earthquake was one of the largest seismic events of the first quarter of the 21st century. It was preceded by a smaller earthquake on July 20 with magnitude 1.4 units lower, and its epicenter was located near that of the July 29 mainshock. Both events were processed with the added stochastic noise version of the WCC method. Three new events were found in a 420-second interval between the mainshock and the first aftershock on July 20. Six new events were found during the 600 second period following the mainshock on July 29. The other events are distributed in location and origin time over the interval. Their depths are within the upper 100 km and body wave magnitude varies from 5.09 to 5.94. The statistical significance of these new events is determined by association of the closest regional stations PETK, JKA, SEY, MA2 as well as the BVAR, KURK, and FINES teleseismic arrays, most sensitive to the Kamchatka region. These stations have the highest statistical weights in the LA process.

The initial findings reported in this paper are also of interest for the further development of the WCC-based methods for detection and phase association. There are several ways to extend the range of objects that can be analyzed. Aftershock sequences from the largest events can be reassessed in terms of the magnitude detection thresholds, more accurate locations of the event hypotheses and the estimation of the relative magnitudes for aftershocks. This direction will allow us to find more events during periods of elevated noise. A second direction aims to study of the smallest possible seismic sources before earthquakes of various sizes. It could help us better understand the process of earthquake preparation [*Schaff et al.*, 2025]. Similar to the study of low-magnitude seismicity before the larger earthquakes, there is a problem related to seismic observations in regions with weak seismicity. These regions do not attract much attention because seismic hazard is low and the data are scarce. The study of regional seismicity in such areas is challenging for the WCC approach and also has potential importance for the future industrial development. There are many global and regional seismic networks [*Gvishiani et al.*, 2024] which can

provide additional data allowing the extension of current study and to reduce the detection threshold in the areas of interest.

Acknowledgments. This work was funded by the Russian Science Foundation (project No. 25-17-00106).

References

Adushkin V. V., Kitov I. O. and Sanina I. A. Further Development of the Matched Filter Method for Solving Seismological Problems // Doklady Earth Sciences. — 2025. — Vol. 523, no. 1. — https://doi.org/10.1134/s1028334x25606182

Arrowsmith S. J. and Eisner L. A technique for identifying microseismic multiplets and application to the Valhall field, North Sea // Geophysics. — 2006. — Vol. 71, no. 2. — P. 31–40. — https://doi.org/10.1190/1.2187804

Baisch S., Ceranna L. and Harjes H.-P. Earthquake Cluster: What Can We Learn from Waveform Similarity? // Bulletin of the Seismological Society of America. — 2008. — Vol. 98, no. 6. — P. 2806–2814. — https://doi.org/10.1785/0120080018

Bobrov D., Kitov I. and Zerbo L. Perspectives of Cross-Correlation in Seismic Monitoring at the International Data Centre // Pure and Applied Geophysics. — 2014. — Vol. 171, no. 3–5. — P. 439–468. — https://doi.org/10.1007/s00024-012-0626-x

Bobrov D. I., Kitov I. O., Rozhkov M. V., et al. Towards global seismic monitoring of underground nuclear explosions using waveform cross correlation. Part I: Grand master events // Seismic Instruments. — 2016a. — Vol. 52, no. 1. — P. 43–59. — https://doi.org/10.3103/s0747923916010035

Bobrov D. I., Kitov I. O., Rozhkov M. V., et al. Towards global seismic monitoring of underground nuclear explosions using waveform cross correlation. Part II: Synthetic master events // Seismic Instruments. — 2016b. — Vol. 52, no. 3. — P. 207–223. — https://doi.org/10.3103/s0747923916030038

Coyne J., Bobrov D., Bormann P., et al. CTBTO: Goals, Networks, Data Analysis and Data Availability // New Manual of Seismological Observatory Practice 2 (NMSOP2). — Deutsches GeoForschungsZentrum GFZ, 2012. — https://doi.org/10.2312/GFZ.NMSOP-2_CH15

Gvishiani A. D., Dzeranov B. V., Skorkina A. A., et al. World Seismic Networks and Earthquake Catalogs // Russian Journal of Earth Sciences. — 2024. — Vol. 24. — ES1012. — https://doi.org/10.2205/2024es000901 — (In Russian).

ISC Bulletin. — 2026. — https://doi.org/10.31905/D808B830

Israelsson H. Correlation of waveforms from closely spaced regional events // Bulletin of the Seismological Society of America. — 1990. — Vol. 80, 6B. — P. 2177–2193. — https://doi.org/10.1785/BSSA08006B2177

Joswig M. Pattern recognition for earthquake detection // Bulletin of the Seismological Society of America. — 1990. — Vol. 80, no. 1. — P. 170–186. — https://doi.org/10.1785/BSSA0800010170

Kennett B. L. N., Engdahl E. R. and Buland R. Constraints on seismic velocities in the Earth from traveltimes // Geophysical Journal International. — 1995. — Vol. 122, no. 1. — P. 108–124. — https://doi.org/10.1111/j.1365-246x.1995.tb03540.x

Kitov I. Cross-correlation Standard Event List of Seismic Activity between the Mainshock and the First Aftershock of the Kamchatka Earthquake on July 29 2025. — 2026. — https://doi.org/10.31905/awqbgagq

Savage J. C. The stopping phase on seismograms // Bulletin of the Seismological Society of America. — 1965. — Vol. 55, no. 1. — P. 47–58. — https://doi.org/10.1785/BSSA0550010047

Schaff D. P., Kim W.-Y. and Richards P. G. Background Seismicity for parts of the northern Korean peninsula // SnT2025. CTBT: Science and Technology Conference. — Vienna, Austria : CTBTO, 2025.

Schaff D. P. and Richards P. G. Repeating Seismic Events in China // Science. — 2004. — Vol. 303, no. 5661. — P. 1176–1178. — https://doi.org/10.1126/science.1093422

Schweitzer J., Fyen J., Mykkeltveit S., et al. Seismic Arrays // New Manual of Seismological Observatory Practice 2 (NMSOP2). — Deutsches GeoForschungsZentrum GFZ, 2012. — https://doi.org/10.2312/GFZ.NMSOP-2_CH9

Sultanov J. J. The role of G. A. Gamburtsev in creating a seismic monitoring method for nuclear testing // Grigory Aleksandrovich Gamburtsev (1903-1955): Memories, essays, articles. — M. : OIFZ RAN, 1998. — P. 188–193. — (In Russian).

Turin G. L. An introduction to matched filters // IRE Transactions on Information Theory. — 1960. — Vol. 6, no. 3. — P. 311–329. — https://doi.org/10.1109/tit.1960.1057571